



Citation for published version:

Rhead, AT, Butler, R & Baker, N 2011, 'Analysis and compression testing of laminates optimised for damage tolerance', *Applied Composite Materials*, vol. 18, no. 1, pp. 85-100. <https://doi.org/10.1007/s10443-010-9153-z>

DOI:

[10.1007/s10443-010-9153-z](https://doi.org/10.1007/s10443-010-9153-z)

Publication date:

2011

[Link to publication](#)

The original publication is available at www.springerlink.com

University of Bath

Alternative formats

If you require this document in an alternative format, please contact:
openaccess@bath.ac.uk

General rights

Copyright and moral rights for the publications made accessible in the public portal are retained by the authors and/or other copyright owners and it is a condition of accessing publications that users recognise and abide by the legal requirements associated with these rights.

Take down policy

If you believe that this document breaches copyright please contact us providing details, and we will remove access to the work immediately and investigate your claim.

ANALYSIS AND COMPRESSION TESTING OF LAMINATES OPTIMISED FOR DAMAGE TOLERANCE

A. T. Rhead • R. Butler • N. Baker

Abstract Barely Visible Impact Damage (BVID) can occur when laminated composite material is subject to out-of-plane impact loads and can result in a significant reduction in compressive strength. This paper will report on compression testing of laminates optimised to maximise damage tolerance. Results from these tests were analysed using a semi-analytical, fracture mechanics based method that predicts the strain below which laminated coupons containing BVID subject to axial compression will not fail. Results from the two optimised stacking sequences considered show an increase of up to 43% in Compression After Impact (CAI) strength in comparison to a baseline configuration. Analysis of results has indicated that CAI strength is dependent to a great extent on damage morphology and stability of damage growth, both of which are functions of laminate stacking sequence.

Keywords Static strength · Delamination · Compression · Impact · Damage tolerance.

1. Introduction

Carbon fibre reinforced plastics (CFRP) are becoming the material of choice for aircraft designers. As has been popularly reported for a number of years, CFRP has the potential to radically reduce the weight of any vehicle in which it is employed. However, this weight saving is not being fully realised even in the latest aircraft such as the Boeing 787 and the Airbus A380. There are a number of reasons for this; one of the most significant being Barely Visible Impact Damage (BVID) and the conservative regulations relating to its in service management.

When layered structures are impacted delaminations can occur which can reduce their static strength by more than 60%. At present the propagation of BVID is suppressed in design by applying empirically derived conservative limits for allowable stress and strain at ultimate levels of load. This is due to an inherent difficulty in in-service detection of BVID. Consequently, regulations for aircraft manufacture effectively state that, provided the level of impact required to cause BVID is due to a “realistically expected event” (defined as a probability of occurrence of 1 in 10^5 flying hours) it must be assumed that such BVID is present and that the structure must tolerate this damage at ultimate levels of load without failing. A computationally efficient analytical model derived in [1, 2] uses a simple approximation of BVID

A. T. Rhead • R. Butler • N. Baker

Department of Mechanical Engineering, University of Bath, Claverton Down, Bath
BA2 7AY, UK

email:R.Butler@bath.ac.uk

morphology along with fracture mechanics applied to a given laminate stacking sequence to predict the threshold strain below which initiation of damage propagation does not occur. This threshold strain is taken as a lower bound to the Compression After Impact (CAI) strength of simple composite structures containing BVID. The model has been applied successfully to a variety of problems from the literature, see [1, 2, 3]. In [1] certain laminate properties that would be desirable for damage tolerant structures and an adaptation of the CAI model allowing determination of the stability of delamination growth were derived. Both are briefly discussed in Section 2.

This paper will focus on a recent series of experiments on two particular stacking sequences that have been derived based on the optimisation principles derived in [1]. These laminates, together with a control coupon were impacted and then loaded in compression until failure. Results of these experiments indicate large increases in static strength can be produced and that the model is capable of making qualitative predictions about the compression after impact (CAI) strength of composite laminates. Detailed C-scan information collected during the course of these experiments has allowed an improved representation of BVID to be employed which has increased accuracy in comparison to the initial approximation to damage morphology.

2. Compression after impact modelling

A brief derivation of the model, including the key assumptions, equations and concepts, is given here. Full derivations are available elsewhere [1, 2]. The model, which is similar to one derived in [4], calculates the threshold strain ε_{th} below which propagation of the delamination damage will not initiate. The central concept of the derivation is to find the difference in energy in the post-buckled sublaminates immediately before, Fig. 1 (a), and after, Fig. 1 (b), the growth of a delamination and to compare this difference to the Mode I fracture energy required to create a new unit of delamination. If sufficient energy is available then a new unit of delamination is created and propagation of the delamination will occur. A thin-film assumption is made that has the effect of allowing no energy to be released from the lower unbuckled region of Figs. 1 (a) and (b). Note that l is the diameter of the sublaminates immediately before propagation, and δl is an infinitesimal length associated with the change in diameter due to propagation.

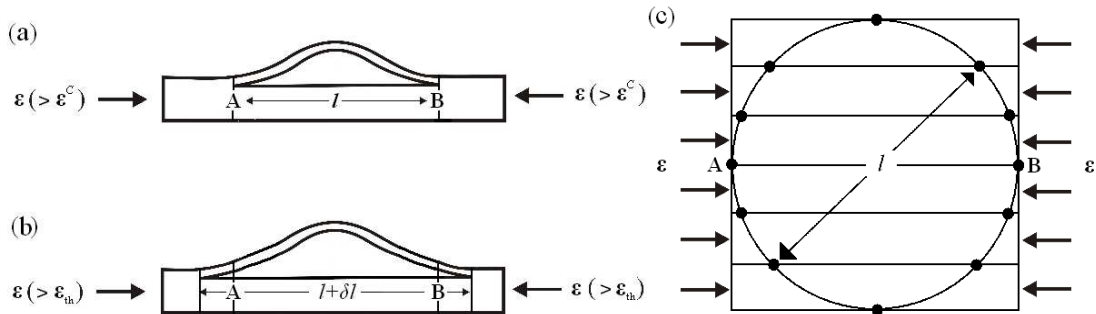


Fig. 1. Thin film model showing; (a) post buckled central section through AB, (b) propagated central section (c), plan view of circular delaminated plate of diameter l with nodes and strips to illustrate the strip discretisation applied for VICONOPT analysis.

Although this change in diameter l is shown along AB in Figs. 1 (a) and (b), it relates to any change in l releasing Mode I fracture energy as is displayed on Fig. 1 (c). The modelling methodology is divided into three parts; damage modelling, delamination buckling and propagation. Each is dealt with in turn in the following subsections.

2.1 Damage modelling

The model requires the calculation of the buckling strain ε^C of a delaminated circular region which is dependent on establishing an approximation to the complex damage morphology resulting from BVID. The model is applied at each possible interface in turn up to a depth of 20% of the total thickness away from the face of the laminate. At each application it is assumed that only the delamination being examined is present in the laminate. Each delamination is approximated by a circle, see Fig. 1(c), with individual delamination diameters being calculated using either of the following two damage models. In the Linear Damage Model (LDM), see Fig. 2, diameters are scaled linearly to a maximum delamination diameter l_{max} (determined from C-scan data, and occurring at approximately 20% of laminate thickness) from l_b , at the outermost interface where,

$$l_b = \frac{7d}{12} \quad (1)$$

and d is the diameter of the tup used to impact the laminate. Whereas the Experimental Damage Model (EDM) uses accurate C-scan information to provide more precise delamination diameters for individual interfaces. This is accomplished by approximating the local damage at each interface by a circle containing the local damage area. In particular, the largest delamination is placed at the correct level which can produce improvements in accuracy compared with the LDM. (Note that the EDM can be conservative as individual delamination diameters are chosen so as to contain the full area of delamination within a circle. This can result in a much larger circular area than a C-scan image of the damage suggests which can lead to reduced delamination buckling strains).

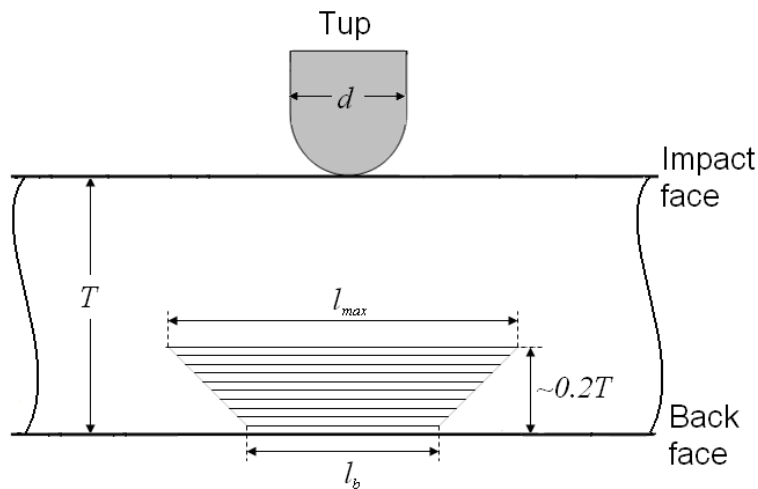


Fig. 2. Cross section of through thickness damage diameter distribution assumed by Linear Damage Model.

2.2 Delamination buckling

Having established a set distribution of damage diameters, the process of calculating ε^C is completed using the composite buckling program VICONOPT [5]. In essence, the delaminated sublaminates are modelled as a thin film such that the boundary along the circular perimeter of the delamination is assumed to be clamped. The program models the circular sublaminates as a series of finite strips, the edges of which are constrained by nodes approximating a circular boundary, see Fig. 1(c). For the results presented later, 6 equal width strips were used with 12 constrained nodes at the junction of these strips and the circular boundary (for the effect of altering number of strips, nodes and constraints see [2]). The strips are then loaded according to the loads applied to the thin film by axial compression of the full laminate. Here, constrained implies that no buckling displacement or rotation is allowed at the nodes, thus approximating a fully clamped boundary. It should be noted that VICONOPT buckling analysis is fully general and can analyse the complex unbalanced and asymmetric sublaminates that can arise in the delaminated sublaminates.

2.3 Propagation

The propagation model is applied at each possible interface in turn up to a depth of 20% of the total thickness away from the back face of the laminate. Hwang and Liu [6] note that for the case of enclosed delaminations, multiple delaminations which are representative of impact damage, can be approximated by a single delamination at a critical interface. Thus at each application it is assumed that only the delamination being examined is present in the laminate and that all secondary effects (i.e. friction between delaminated layers) relating to multiple delaminations being present in the laminate are ignored. The post buckled sublaminates, i.e., the thin buckled region in Figs. 1 (a) and (b), is considered to contain bending energy and membrane energy. In order to calculate the energy due to bending it is assumed that the energy stored exactly equals the applied in-plane energy [7]. Hence the application of a simple work done equation gives,

$$U_1(l) = A_{11}l(\varepsilon - \varepsilon^C)\varepsilon^C \quad (2)$$

Note here that ε is the applied strain under displacement control and A_{11} is the axial stiffness of the sublaminates. Note also that the term $(\varepsilon - \varepsilon^C)$ implies bending energy is not stored in the sublaminates until after buckling has occurred.

Following [7, p.171] a simplified membrane energy associated with the sublaminates before buckling occurs is given by,

$$U_2(l) = \frac{A_{11}}{2}l(\varepsilon^C)^2 \quad (3)$$

The above equations describe the energy available in the sublaminates prior to propagation. However, energy for propagation is also available in the form of membrane energy released from the section of the sublaminates of length δl which becomes delaminated during propagation. This energy is calculated using,

$$U_2^* = \frac{A_{11}}{2} \int_0^{\delta l} \varepsilon^2 dx \quad (4)$$

The bending and membrane energy in the sublaminates immediately after propagation occurs can be calculated by replacing l with $l + \delta l$ in Eqs. (2) and (3). Finally, it remains to compare energies before and after propagation to determine whether there is sufficient energy to cause propagation. Eq. (5) and a comparison of buckling strains before and after propagation are employed to give this comparison at the instant propagation occurs. Here G_I is the Mode I strain energy release rate (SERR).

$$G_I = \lim_{\delta l \rightarrow 0} \{U_1(l) - U_1(l + \delta l) + U_2(l) - U_2(l + \delta l) + U_2^*\} \frac{1}{\delta l} \quad (5)$$

Hence

$$G_I = \frac{A_{11}}{2} (\varepsilon - \varepsilon^C)(\varepsilon + 3\varepsilon^C) \quad (6)$$

By comparing this value to G_{IC} , the SERR required to cause Mode I failure of the resin, it is possible to determine whether propagation will occur at this level of strain. If the above equation is rearranged and G_I is set equal to G_{IC} it is possible to calculate the threshold strain, when $\varepsilon = \varepsilon_{th}$, i.e.

$$\varepsilon_{th} = \varepsilon^C \left(\sqrt{4 + \frac{2G_{IC}}{(\varepsilon^C)^2 A_{11}}} - 1 \right) \quad (7)$$

The sublaminates at which the lowest threshold strain for propagation is determined will be the first to propagate. Note that for simplicity, the assumption is made (see [2]) that propagation initiates under Mode I conditions in the direction of applied strain ε .

The model determines the interface at which propagation will first occur. However, propagation at other interfaces may be required to cause final failure, particularly when growth at the first interface is shown to be stable. Briefly, a sublaminates growth stability i.e. whether, growth only occurs gradually with increasing strain (stable growth) or whether once a critical strain is reached, propagation continues without an increase in strain being required (unstable growth) can be determined from Eq. (6) by the inequality,

$$\frac{\varepsilon_{th}}{\varepsilon^C} \geq 3 \quad (8)$$

If the inequality holds, growth is stable. The equality in Eq. (8) is the maximum of the curve defined by Eq. (6) for $\varepsilon = \varepsilon_{th}$ and fixed A_{11} i.e. a fixed sublaminates. The inequality is determined by considering the change in G_I due to a change in l and hence ε^C following propagation. If, following propagation at a fixed strain $\varepsilon = \varepsilon_{th}$, G_I is greater than or equal to G_{IC} then propagation will continue without an increased load. Thus every interface created by delamination is analysed to determine at what level of strain propagation occurs and whether or not this growth is stable.

2.4 Laminate optimisation

The above model is a combination of the four variables ε^C , ε , A_{11} and G_I . As such it describes a 4D surface. Although it is difficult to extract useful information directly

from this 4D surface, it is possible to fix one or more of the variables at an appropriate value (usually at $\varepsilon = \varepsilon^{th}$ or $G_I = G_{IC}$) to create 2D or 3D surfaces which are much easier to interpret. Figure 3 shows a 3D surface created by fixing $G_I = G_{IC}$. This surface allows all possible sub-laminates, which are defined by A_{11} and ε^C with regard to the initiation model, to be compared and hence some optimal features to be identified.

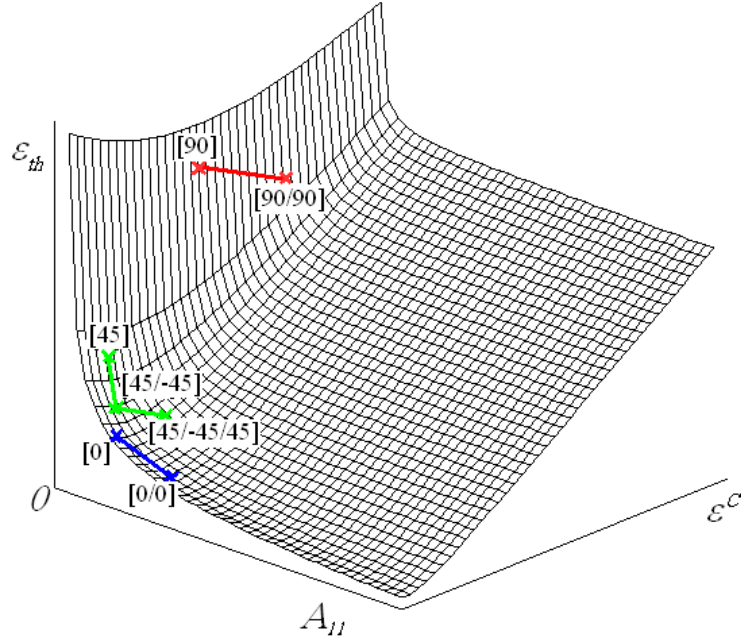


Fig. 3. 3D surface created by fixing $G_I = G_{IC}$ in Eq. (7) Also plotted are five sub-laminates made from AS4/8552 material.

With the objective of optimising threshold strain, and hence maximising CAI strength, it is quite clear from Fig. 3 that this can be accomplished by minimising A_{11} and maximising ε^C . Figure 3 shows the position on the surface of 7 theoretical sub-laminates of a quasi-isotropic laminate made from the AS4/8552 material described below. The sub-laminates highlighted on Fig. 3 have equal damage area and as such their associated threshold strains are directly comparable. Noting this, the sub-laminates made from 90° layers or 45° layers are obviously more optimal than those made from 0° layers as the former offer lower A_{11} and higher ε^C . Using the above, two stacking sequences have been identified as possible candidates for a damage tolerant quasi-isotropic laminate, see Table 1.

Table 1.
Stacking sequences for coupons.

Material (Laminate ID)	Lay-up
AS4/8552 (Control)	$[45,0,-45,90]_{4S}$
AS4/8552 (45° Outer)	$[(45,-45)_4,(90,0)_4]_S$
AS4/8552 (90° Outer (1)) and (90° Outer (2))	$[90_3,45,90,-45_3,0,45_3,0_2,-45,0]_S$

The first, $[(45,-45)_4,(90,0)_4]_S$, was a product of the authors' experience which mimics current design philosophies for prevention of global buckling (placing $\pm 45^\circ$ layers to

the outside of the laminate) whilst also exploring the damage tolerance properties of this configuration. The idea of placing $\pm 45^\circ$ plies in the surface layers have also been investigated by Hitchen and Kemp [9] who observed an increase in damage tolerance. The second, $[90_3, 45, 90, -45_3, 0, 45_3, 0_2, -45, 0]_S$, was a product of an optimisation routine described in [8] which sought to minimise angles between plies (to improve damage resistance) and minimise A_{11} for the outermost layers while following current design constraints regarding blocking of a maximum of three plies to prevent intraply cracking.

3. Experimental method

Quasi-isotropic coupons were made from Hexcel AS4/8552 pre-preg layers with material properties given in Table 2 and stacking sequences given in Table 1. Samples were cured in an LBBC Quicklock Thermoclave using the Hexcel specified curing cycle. Coupons were tabbed with 1.5mm aluminium plates to provide grip and to prevent crushing at the loading points.

Table 2.
Material properties. t is layer thickness.

Material	E_{11} (GPa)	E_{22} (GPa)	G_{12} (GPa)	ν_{12}	t (mm)	G_{1C} (J/m ²)
AS4/8552	128.0	10.3	6.0	0.3	0.125	261

As indicated on Fig. 4 the coupons were subjected to 8J single out-of-plane impacts at their (plan form) centre. The impacts were delivered using an Instron Dynatup 9250HV instrumented impact tester employing a hemispherical tup with a 16mm diameter. The impact tester has a pneumatic anti-bounce mechanism that catches the tup after initial impact thereby ensuring the coupons were impacted only once. During impact coupons were clamped over a 75 mm x 125 mm window cut into a steel base as prescribed by the ASTM standard [10]. The coupons were orientated such that the long edge of the coupon was parallel to the long edge of the test window. The extent of BVID was measured using an Ultrasonic Sciences C-scan system.

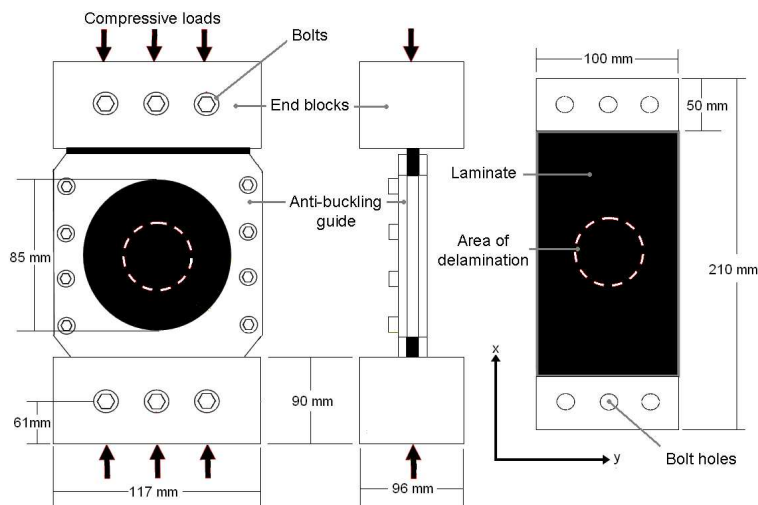


Fig. 4. Experimental set-up and coupon details.

Axial compressive load was applied under displacement control at 0.1 mm/min, using an Instron 5585H test machine, until failure. An anti-buckling guide with a circular window 85 mm in diameter was used in order to prevent global buckling including any global/local interaction and to ensure samples failed by damage propagation following delamination buckling.

Strains were recorded throughout the tests by two pairs of back-to-back strain gauges attached to a HBM 600 Hz Spider 8 data acquisition system. The back (non-impact) faces of the coupons were covered in a random speckle pattern to allow images and video to be captured of buckling modes and final failure sequences using a Limes VICONOPT VIC-3D HS Digital Image Correlation (DIC) system. This system employs Photron Fastcam SA3 cameras capable of 2000 frames per second (fps) at full resolution. Coupons, end fixtures and anti-buckling guides are described in Fig. 4.

4. Results

Experimental and analytical strains are given together with VICONOPT buckling strains and critical sublaminates in Table 3 for all interfaces/sublaminates of interest i.e. those that have the potential to show some delamination growth behaviour. Data obtained from the C-scan system was used to produce colour plots showing qualitative through thickness position of delaminations as seen in Fig. 5 for use in the Experimental Damage Model (EDM).

Table 3.
Analytical buckling and propagation strains for critical sublaminates using the Linear and Experimental Damage Models (LDM and EDM) compared with experimental propagation strains.

Laminate ID	Critical Sublaminates		Buckling (μ strain)		Propagation (μ strain)		
	EDM	LDM	EDM	LDM	EDM	LDM	Experimental
Control	(45,0)	-	1796	-	4310	-	5700
	(45,0,-45)	(45,0,-45)	3346	1143	4742	3834	5700
	(45,0,-45,90)	-	3709	-	4874	-	5700
45° Outer	(45,-45)	-	1904	-	6081	-	5882**
	(45,-45,45)	-	5874	-	7198	-	7350***
	-	(45,-45) ₃	-	4037	-	4997	5882**
90° Outer (1)	(90 ₃ ,45)	-	3014	-	6637	-	6400
	-	(90 ₃ ,45, 90)*	-	6430	-	8238	6400
90° Outer (2)	(90 ₃ ,45)	-	3086	-	6656	-	6200
	-	(90 ₃ ,45, 90)*	-	6576	-	8349	6200

*The LDM actually gives a lower strain at the 6th level but this is disregarded as it occurs at a -45/-45 interface at which (due to fibre bridging) delamination will not occur.

** Initial stable propagation only.

***Final unstable failure.

A summary of experimental stresses, calculated by dividing failure load by cross sectional area, are given in Table 4 with individual coupon thicknesses and percentage increases in experimental stress for the optimised coupons over the Control coupon.

Table 4.
Individual coupon thickness, failure stress and percentage strength increase.

Material (Laminate ID)	Coupon Thickness (mm)	σ_{failure} (MPa)	σ_{failure} increase over Control (%)
AS4/8552 (Control)	4.39	244	0
AS4/8552 (45° Outer)	4.29	349	43
AS4/8552 (90° Outer (1))	4.35	264	8
AS4/8552 (90° Outer (2))	4.36	273	12

4.1 Control Laminate-[45,0,-45,90]_{4S}

Figure 5(a) shows the C-scan image before the CAI test, from which the smallest circle containing the full damage area was measured as having $l_{\text{max}} = 36\text{mm}$. However, careful inspection of the C-scan image revealed that (unlike the other laminates tested) no delamination at a single interface spanned the entire width of the damage circle defined by l_{max} .

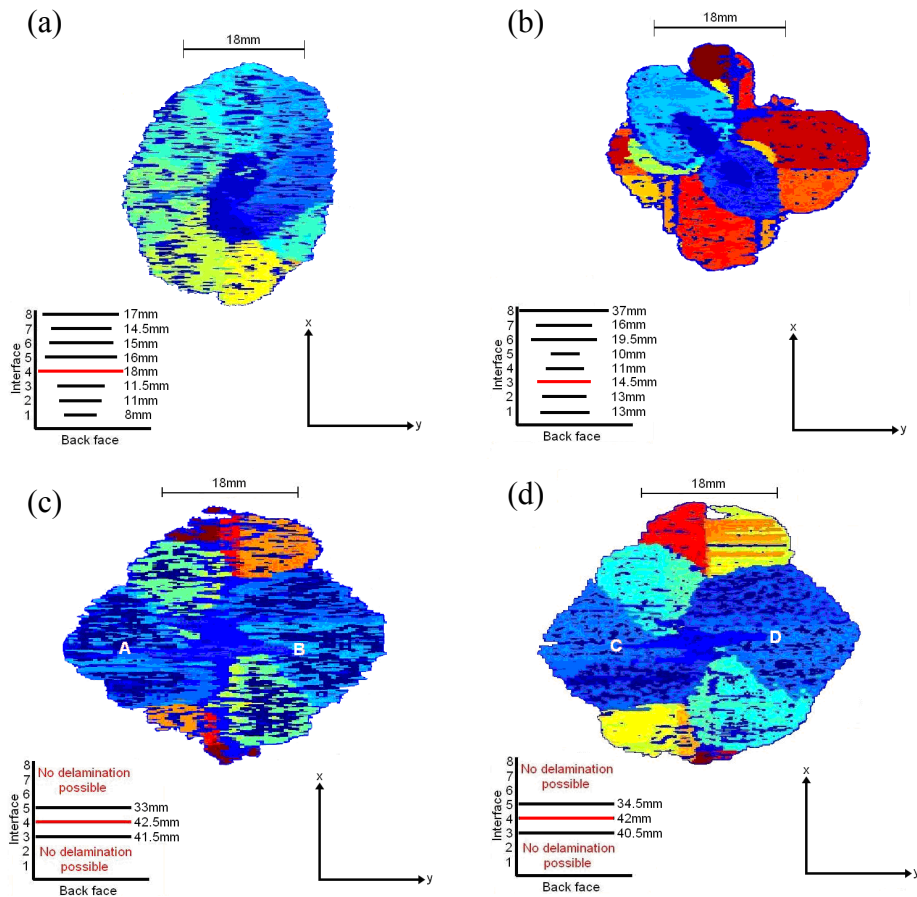


Fig. 5: Ultrasonic C-scan images of BVID with insets showing EDM representations from the back face of (a) the Control, (b) 45° Outer, (c) 90° Outer (1), and (d) 90° Outer (2) coupons.

The divergence in strain gauge readings at 50-60 kN (see Fig. 6(a)) was related to an initial imperfection in coupon alignment which lead to bending in the test piece which was arrested between 80-90 kN via contact with the anti-buckling guide. Figure 6 (a) indicates delamination buckling occurred at approximately 33-40 kN. Careful study of gauges 2 and 4 shows some limited change in stiffness at approximately 65-75kN which may be related to further delamination buckling. Table 3 gives the experimental final failure strain corresponding to a failure load of 107 kN, equivalent to a stress of 244 MPa. For the purposes of the EDM the damage diameter at the critical level was 18mm.

4.2 45° Outer Laminate-[(45,-45)₄,(90,0)₄]_s

Figure 5(b) shows the C-scan image before the CAI test from which it can be determined that $l_{max} = 37\text{mm}$. Table 3 gives a nominal experimental propagation strain of 5882 μstrain corresponding to an applied load of 120 kN. As for the Control laminate, Fig. 6(b) shows that divergence in strain gauge readings at 40-50 kN was related to an initial imperfection in coupon alignment which lead to bending in the test piece which was arrested between 70-80 kN via contact with the anti-buckling guide. Additionally, Fig. 6 (b) indicates delamination buckling occurred at approximately 38kN. For the purposes of the EDM the damage diameter at the critical level was 14.5mm, see Fig. 5(b).

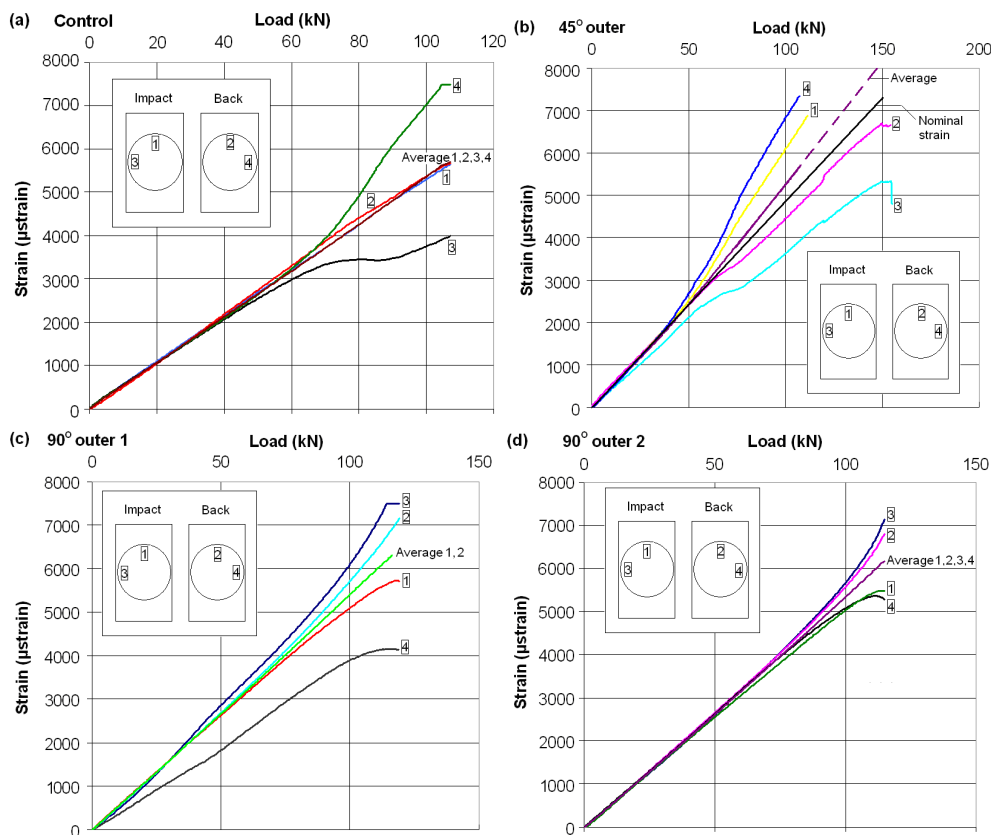


Fig. 6. Strain vs. Load plots for the four coupons with inset showing strain gauge positions: (a) Control, (b) 45° Outer, (c) 90° Outer (1) and (d) 90° Outer (2).

Gauges 1 and 4 reach the maximum strain that can be input to the data acquisition system at 107 and 111 kN respectively after which the strain was not recorded. Hence the projected average strain from this point (dotted line) is continued with the same gradient. Kinks in gauges 2 and 3 at 120 kN indicate occurrence of a damage propagation event. Final failure occurred at 150 kN (equivalent to a nominal strain of 7350 μ strain and stress of 349 MPa) due to transverse full width cracking; although post compression C-scan images clearly show damage propagation in the four principal fibre directions.

4.3 90° Outer (1) Laminate-[90₃,45,90,-45₃,0,45₃,0₂,-45,0]_s

Figure 5(c) shows the C-scan image before the CAI test giving $l_{\max} = 42.5\text{mm}$. An intraply crack 3 layers deep, a result of impact, runs from point A to B on Fig. 5(c) and was a factor in final failure of the laminate. Gauges 1 and 2 on Fig. 6 (c) show delamination buckling occurs at approximately 40-50 kN. Table 3 gives the experimental failure strain corresponding to a load of 119 kN and a stress of 264 MPa. For the purposes of the EDM the damage diameter at the critical level was 42.5mm.

4.4 90° Outer (2) Laminate-[90₃,45,90,-45₃,0,45₃,0₂,-45,0]_s

Figure 5(d) shows the C-scan image before the CAI test giving $l_{\max} = 42\text{mm}$. An intraply crack 3 layers deep runs from point C to D and was a factor in final failure of the laminate. Figure 6 (d) shows delamination buckling occurred at approximately 44-50 kN. Table 3 gives the experimental final failure strain corresponding to a failure load of 115 kN (and a stress of 273 MPa) as shown in Fig. 6(d). For the purposes of the EDM the damage diameter at the critical level was 42mm. 3D plots and cross-sections showing out of plane displacement from the DIC system (Fig. 7) indicated a delamination propagation event occurred shortly before transverse full width cracking caused final failure.

5. Discussion

5.1 Impact damage

As noted in Section 4, inspection of the C-scan image of the Control coupon revealed that (unlike the other laminates tested) no delamination at a single interface spanned the entire width of the damage circle defined by l_{\max} . This is because the angle between adjacent layers is 45° which disperses damage throughout the laminate, making the laminate damage resistant.

A visual inspection of the impacted coupons revealed that both 90° Outer laminates had large intraply cracks through the non-impact outer layers which almost certainly had a negative effect on the strength of the laminate. In addition, Figs. 5 (c) and (d) show the two 90° Outer laminates had almost identical damage morphologies. During impact the limited possible interfaces (due to ply blocking) at which delamination could occur in these coupons resulted in impact energy being dispersed over a smaller number of interfaces and hence the area of each delamination was larger than expected.

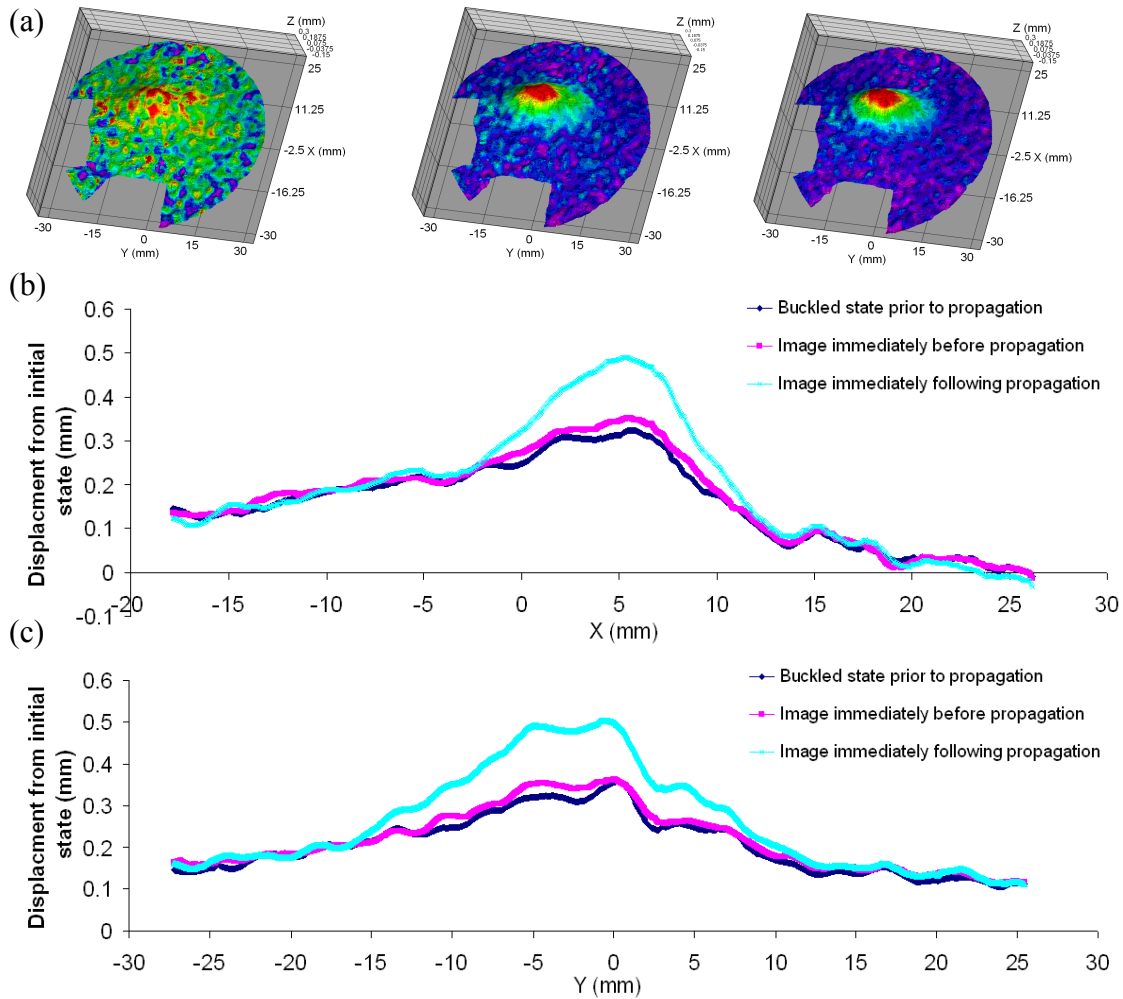


Fig. 7. (a) Three consecutive DIC images of the 90° Outer (2) coupon taken at 50 fps demonstrate a propagation event occurred by showing displacement from an earlier buckled state. (b) and (c) show DIC cross-sections through the peak of the buckle, parallel and perpendicular to the loading direction respectively.

The outcome of this was that buckling strains and therefore threshold strains were reduced which in turn produced a weaker laminate than predicted by the optimisation strategy which assumed the linear (LDM) damage distribution shown in Fig. 2. The performance of the 90° Outer coupons could also have been affected by the ASTM rectangular impact test window [10] over which coupons were placed during impact. The rectangular shape reduced the length over which 90° fibres bent during impact which in turn increased their bending stiffness when compared to the 0° fibres. This caused larger delaminations than assumed by the LDM (and larger than would probably occur in service) to occur closer to the back face (where bending forces peak during impact) thus resulting in an earlier failure than if impact had been over a square window.

Analysis of the C-scan output for the 90° Outer coupons shows that the largest delamination was between the 4th and 5th layers. This is an obviously weak interface where stress is likely to be concentrated during impact loading. Similarly, the stacking sequence for the 45° Outer coupon indicates a large delamination should be present between the $\pm 45^\circ$ fibres and $90^\circ/0^\circ$ fibres (8th ply interface) and this is indeed

confirmed to be the case by the C-scan images in Fig. 5. However, in contrast to the effect on the 90° Outer coupons, the weak 8th interface in the 45° Outer coupons is thought to have significantly increased its CAI strength. It is assumed by the authors that the depth of the weak interface in the 45° Outer coupon and the fact that a large area of damage was ‘drawn’ to it away from the critical damage region (approximately 5-20% of laminate thickness) was a major contributing factor to the high strength of the laminate. This may be a factor to consider in future optimisation strategies.

5.2 Compression testing

Divergence in strain gauge readings at medium levels of load for the Control, 45° Outer and 90° Outer (1) coupons is attributed to an initial imperfection leading to compression induced bending which is then arrested by contact with the anti-buckling guide as can be seen in Fig. 6. Strain gauge readings in Fig. 6 indicate that the limited bending that occurred placed the back face on the Control and 45° Outer coupons under increased compression which may have reduced their failure load. Readings from the strain gauges for the 90° Outer (1) coupon show bending also occurred for this coupon although the back face was placed in increased tension which may have increased buckling resistance and hence failure load in this case. Figure 6 (d) shows no bending was detected in the 90° Outer (2) coupon. Results presented in Figs. 5 and 6 together with further DIC information (similar to the images seen in Fig. 7), not presented here for brevity, indicate that all laminates failed as a result of propagation of damage following delamination buckling.

Delamination buckling strains were predicted by VICONOPT in combination with EDM to an acceptable tolerance. In the case of the Control coupon initial delamination buckling of the two layer sublaminates was predicted to occur at 1796 μ strain with experimental buckling shown to occur in the region of 1800-2200 μ strain. Buckling of the 3 and 4 layer sublaminates is predicted to occur at the same level of strain that bending of the full coupon occurs making local buckling difficult to detect although, as noted in Section 4.1, gauges 2 and 4 appear to show a change in stiffness which may be attributed to sublaminates buckling. Figure 6 (b) shows that initial sublaminates buckling in the 45° Outer coupon occurs at approximately 2000 μ strain which is well predicted by the buckling model for the 2 layer sublaminates, see Table 3. Buckling of the 3 layer sublaminates is predicted by VICONOPT to occur at 5874 μ strain however, this coincides with an obvious propagation event as seen in Fig. 6 (b) hence no local buckling was detected by the strain gauges. Sublaminates buckling strains are marginally over predicted by VICONOPT for the 90° Outer coupons with buckling occurring in the region of 2400-2600 μ strain for the 90° Outer (1) coupon and in the region of 2500-2700 μ strain for the 90° Outer (2) coupon. Note that cross-sections in Fig. 7 show that a second propagation occurred immediately prior to final failure.

Results of the compression tests in Table 4 show that the 90° Outer coupons produced an average improvement in strength over the control laminate of 10% whereas the 45° Outer laminate showed an improvement of 43%.

5.3 Comparison of experimental and analytical propagation

Table 3 shows that the LDM analytical results differ from the experimental strain results by 33%, 32%, 29% and 35% for the Control, 45° Outer, 90° Outer (1) and 90° Outer (2) respectively. Clearly, as noted above, the LDM does not work well for the

more exotic stacking sequences presented here which include blocks of layers with the same orientation and unusual damage morphologies. This is probably due to the inflexibility of the LDM with regard to position of the largest damage diameter. The lack of prior knowledge, with regard to the damage morphology of individual laminates, is a weakness that was exploited by the optimisation procedure to derive laminates that were only optimal for the LDM damage morphology.

However, analytical results can be improved by careful study of the C-scan images to derive the correct damage diameter for each interface, see Fig. 5, and via an analysis of the buckling strain of and the stability of delamination growth at individual interfaces. Results shown in Table 4 for initial propagation using the EDM differ from the experimental strain values by 17%, 3%, 4% and 7% for the Control, 45° Outer, 90° Outer (1) and 90° Outer (2) laminates respectively. In particular, the EDM analysis using the C-scan data was able to capture the events up to and including failure in the 45° Outer compression test. Application of Eq. (8) shows that growth at the 2nd interface in the 45° Outer coupon, which is thought to be linked to the propagation event at 120 kN, is stable. As the growth at the second level is stable it is unlikely to be the cause of final failure hence propagation of damage at other levels needs to be considered. The level with second lowest propagation strain and hence next to propagate is the unstable 3rd interface with sublaminare lay-up (45,-45,45) which buckles at 5874 μ strain and has a threshold strain of 7198 μ strain. This differs by only 2% from the experimental failure strain.

For the Control coupon, propagation at the 2nd interface (4310 μ strain) is predicted to be briefly unstable before becoming stable which is then followed by unstable growth at the 3rd interface. Due to the inherent difficulty in accurate sizing of individual delamination areas and the effect this has on calculated strains it is quite likely that propagation at the 2nd level is in fact purely stable which would correlate with experimental results. Additionally, buckling strains for individual sublaminae in the Control coupon given in Table 4 show that the sublaminare linked to the third interface buckles at a lower strain (3346 μ strain) than the strain at which damage growth is predicted to occur at the second interface (4310 μ strain). Hence buckling of the three layer sublaminare may stop propagation from occurring at the 2nd interface by causing the buckle to close and thus reducing Mode I effects. Hence, propagation may occur at the third interface where there is an open buckle. The same situation is noted for 3rd and 4th interfaces hence growth may occur at 4874 μ strain at the fourth interface, a difference of 14% in comparison to the experimental result. However, it should be noted that VICONOPT is a linear buckling program that does not calculate the post-buckling behaviour of the individual layers and so could not be relied upon for completely accurate results if a sequence of buckles is considered. It is therefore concluded for conservativeness that the model predicts unstable growth and hence failure at the 3rd interface. Note that it is likely that the lack of stiffness in the sublaminare due to earlier buckling of layers closer to the surface will most likely have reduced the buckling strain of the sublaminare relating to the 4th interface thus resulting in buckling at the 3rd and 4th interfaces being difficult to separate on the plots of strain gauge readings in Fig. 6. Hence sequential buckling of layers should not be ruled out.

6. Conclusions

Experimental results demonstrate increases of 10% and 43% in damage tolerant strain can be achieved by replacing a standard $[45,0,-45,90]_{4S}$ laminate with $[90_3,45,90,-45_3,0,45_3,0_2,-45,0]_S$ and $[(45,-45)_4,(90,0)_4]_S$ laminates, respectively. However, stable propagation of damage was observed before failure in the latter laminate with layers of $\pm 45^\circ$ material outermost. Analysis of the C-scan data from the coupons has led to the conclusion that weak interfaces can exist in stacking sequences and may have both positive and negative effects on laminate strength. It has also been established that blocking of near surface plies, as seen in the 90° Outer coupon, should be avoided.

The results also show that the CAI model is capable in its current form of making qualitative predictions about CAI strength using the Linear Damage Model and so is a legitimate basis for an optimisation routine aimed at improving damage tolerance. However, the optimised stacking sequences have identified a weakness in the damage modelling assumptions. It has been shown that this weakness can be ameliorated by using detailed experimental C-scan data. Clearly, this is not a predictive strategy and so is not applicable to an optimisation procedure. Hence, a key finding that has come from this work, which is supported by Hitchen and Kemp in [9], is that optimisation of laminates for damage tolerance requires a model capable of predicting propagation of given damage but also a model capable of predicting the damage morphology of an impacted laminate. Otherwise, as has been demonstrated, optimisation will frequently produce laminates that are only optimal for the initially suggested damage distribution. Damage tolerance and impact damage morphology are inextricably linked; altering one will alter the other. The same is true of propagation stability. The fact that in the 45° Outer coupon, growth of delaminations between near surface plies is stable rather than unstable is a key component of the improved strength of this laminate and should be considered in future optimisation routines.

Hence future work will centre around an improved optimisation procedure for damage tolerant laminates based on the CAI model while paying attention to growth stability of individual delaminations. As noted a more detailed predictive method for damage morphology may be necessary although it would need to be computationally efficient to maintain the advantage offered by the current methodology. This may be accomplished by producing a method that can identify weak interfaces and/or cause them to occur deeper within the laminate.

Acknowledgements Andrew Rhead is sponsored by the Great Western Research (GWR) alliance and Airbus UK. The authors are grateful to the University of Bristol for providing materials and impact test facilities and Mr. M. Kinawy at the University of Bath for his assistance with impact and compression testing.

References

1. Rhead, A.T., Butler, R., Hunt, G.W.: Post-buckled propagation model for compressive fatigue of impact damaged laminates. *Int. J. Sol. Struct.* **45**(16), 4349-4361 (2008)
2. Rhead, A.T., Butler, R.: Compressive static strength model for impact damaged laminates. *Compos. Sci. Technol.* **69**(14), 2301-2307 (2009)
3. Rhead, A.T., Butler, R., Marchant, D.: Compressive strength of laminates following free edge impact. *Comp. Part A.* (2009). doi:10.1016/j.compositesa.2009.10.024 article in press.
4. Chai, H., Babcock, C.D., Knauss W.G.: One dimensional modelling of failure in laminated plates by delamination buckling. *Int. J. Struct.* **7**(11), 1069-1083 (1981)
5. Williams, F.W., Kennedy, D., Butler, R., Anderson, M.S.: VICONOPT – Program for exact vibration and buckling analysis or design of prismatic plate assemblies. *AIAA*, **29**(11), 1927 - 1928 (1991)

6. Hwang, S.-F., Liu, G.-H.: Buckling behaviour of composite laminates with multiple delaminations under uniaxial compression. *Composite Structures*, **53**, 235-243 (2001)
7. Thompson, J.M.T., Hunt, G.W.: *Elastic Instability Phenomena*. 1st edition, Wiley and Sons, (1984)
8. Baker, N., Rhead, A.T., Butler, R.: Optimisation of aerospace laminates for damage tolerance. 7th ASMO-UK/ISSMO International Conference of Engineering Design Optimisation, Bath (2008)
9. Hitchen, S.A., Kemp, R.M.J.: The effect of stacking sequence on impact damage in a carbon fibre/epoxy composite. *Composites*, **26**, 207-214 (1995)
10. ASTM 2009 Standard test method for measuring the damage resistance of a fiber-reinforced polymer matrix composite to a drop-weight impact event, Designation: D7136 / D7136M - 07
doi:10.1520/D7136_D7136M-07